Karlsruhe Institute of Technology

Electrokinetic optimization of a micro-mixer for lab-on-chip applications

Dominik P.J. Barz
Hendryk Bockelmann
Vincent Heuveline

No. 2012-02

Preprint Series of the Engineering Mathematics and Computing Lab (EMCL)

KIT – University of the State of Baden-Wuerttemberg and
National Research Center of the Helmholtz Association

www.emcl.kit.edu

Preprint Series of the Engineering Mathematics and Computing Lab (EMCL)
ISSN 2191–0693
No. 2012-02

Impressum

Karlsruhe Institute of Technology (KIT)
Engineering Mathematics and Computing Lab (EMCL)

Fritz-Erler-Str. 23, building 01.86
76133 Karlsruhe
Germany

KIT – University of the State of Baden Wuerttemberg and
National Laboratory of the Helmholtz Association

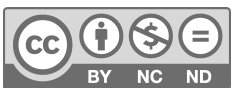

Electrokinetic optimization of a micromixer for lab-on-chip applications

Hendryk Bockelmann and Vincent Heuveline

Karlsruhe Institute of Technology,

Engineering Mathematics and Computing Lab (EMCL),

Fritz-Erler-Str. 23, D-76133 Karlsruhe, Germany

Dominik P.J. Barz*

Queen's University,

Department of Chemical Engineering,

Dupuis Hall 213, Kingston,

Ontario K7L 3N6, Canada

(Dated: January 26, 2012)

Abstract

This paper is concerned with the optimization of an electrokinetic micromixer suitable for Lab-on-Chip and other microfluidic applications. The mixing concept is based on the combination of an alternating electrical excitation applied to a pressure-driven base flow in a meandering microchannel geometry. The electrical excitation induces a secondary electrokinetic velocity component which results in a complex flow field within the meander bends. A mathematical model describing the physicochemical phenomena present within the micromixer is implemented in an in-house Finite-Element-Method code. We first perform simulations comparable to experiments concerned with the investigation of the flow field in the bends. The comparison of simulation and experiment reveals excellent agreement. Hence, the validated model and numerical schemes are employed for a numerical optimization of the micromixer performance. In detail, we optimize the secondary electrokinetic flow by finding the best electrical excitation parameters, i.e. frequency and amplitude, for a given waveform. The simulation results of two optimized electrical excitations featuring a discrete and a continuous waveform are compared and discussed. The results demonstrate that the micromixer is able to achieve high mixing degrees very rapidly.

* dominik.barz@chee.queensu.ca

I. INTRODUCTION

The field of microfluidics comprises the control and manipulation of flows with typical length scales in the range of micrometers and typical volumes in the range of nanoliters. Excellent reviews of such flows are available in references [1–3]. Several versatile technological concepts are based on microfluidics such as Lab-on-Chip (LOC) and micro reaction technology. The Lab-on-Chip concept is unique among microfluidic systems in that it aims for the integration of all unit operations that are required in a (bio-)chemical laboratory on one microfluidic chip of only few square centimeters in size. These steps typically include chemical synthesis or labeling of proteins which require local mixing of reagents. Consequently, the investigation of mixing strategies in microfluidic devices is of particularly great interest. Mixing eventually occurs by diffusion on a molecular level and can therefore only be improved by two approaches: (i) via an enlargement of the (virtual) contact interfaces between the liquids/species to be mixed; and/or (ii) via decreasing of the molecular diffusion path. These features are usually achieved in macroscopic geometries by employing fluid-mechanical instabilities or turbulent flows. Contrary to flows in conventional channels, flows in microscopic channels are typically characterized by small Reynolds numbers in the range of $Re \sim 0.01 - 10$. At these low Reynolds numbers, inertial forces are weak and cannot be engaged to enhance mixing by flow instabilities or turbulence; other means are needed to facilitate mixing. A variety of microfluidic mixing concepts has been proposed in literature. These concepts can principally be separated into two categories: (i) passive methods which are based on suitable micro structures; (ii) active methods which are associated with the introduction of energy into the system.

Many passive mixers take advantage of centrifugal or chaotic (secondary) flows, suitable to increase the contact interface of the liquids. Typical designs are T-mixers with different inlet channel diameters [4] or with J-shaped baffles in the common channel [5], plane hair-pin channels [6] and modified Tesla structures [7]. Other designs include perforated meandering channels [8], bas-relief structures on the channel floors (the so-called herringbone mixer) [9], and three-dimensional serpentine channels [10]. Another passive mixer approach is the multi-lamination concept, i.e. the split-up of liquid streams into thinner lamellas and their subsequent recombination (cf. e.g. [11, 12]). This concept is intended for both large contact areas and short diffusion paths without introducing a secondary flow. Passive methods are

generally linked to manufacturing of rather complex three-dimensional channel geometries and they often require relatively-high Reynolds numbers.

Alternatively, active methods often allow for straightforward channel geometries, however, external forces have to be induced to create a secondary flow component. To date, several concepts have been realized based on different physicochemical phenomena. Ahmed et al. [13] demonstrate fast mixing inside a microfluidic channel due to the acoustic excitation of an air bubble trapped in a cavity. Khatavkar et al. propose a mixing concept based on an array of individually addressable artificial cilia covering the channel wall stirring the surrounding fluid [14]. Another concept by Yi et al. use magnetic forces to stir the liquids by applying a uniform magnetic field in conjunction with steady or time-dependent electrical currents [15]. Mixing as a result of simple low frequency vibration of the microfluidic device is reported by Oberti et al. [16]. The vibrations induce vortices in proximity to sharp corners of the channel junctions.

Various Lab-on-Chip concepts rely on electrokinetic phenomena to realize unit operations, such as liquid pumping [17, 18], analyzing of ions [19], or the manipulation of particles or cells [20, 21]. Electrokinetic phenomena are related to the presence of an electrical double layer (EDL); comprehensive review is given by [22]. Electroosmosis, also called electrokinetic flow, is the motion of a liquid under the influence of an applied electric difference (gradient) relative to a charged solid surface. This electrokinetic phenomenon is a favorable tool to induce flows in microstructures without applying a pressure gradient or the usage of micro-mechanical parts. The utilization of electrokinetic phenomena to improve mixing in micro-flows is described by several authors and, in principle, two different approaches are identified in literature. One approach takes an advantage of an electrokinetic instability in which an oscillating electric potential difference is applied to a layered flow of two liquids with different ionic conductivities [23, 24]. This results in a Coulomb force at the liquid-liquid interface which stretches and folds it and mixing of the electrolytes occurs rapidly. A similar effect is observed under the influence of a steady electric potential difference [25]. The other approach is based on electrokinetic flows of liquids of homogeneous conductivity, whereas the secondary flow regime has to be either created by alternating surface charges (zeta potentials) as shown in [26, 27] or employing appropriate channel geometries [28]. The latter mixer concept relies on the interaction of electrokinetic flow and a meandering

channel segment. A pressure-driven flow drives the layered liquids to be mixed through the meander channel. An oscillating secondary electrokinetic flow, induced by an alternating applied electric potential difference, increases the mixing performance considerably given a reasonable ratio of main flow to secondary flow amplitudes. This approach is attractive in its simplicity since it neither relies on specific ionic liquid properties, nor complicated patterning of a microchannel's surface charges. Additionally, the mixing concept does not require complex microfluidic structures and allows for a straightforward control by manipulating the electrical excitation parameter.

Even though a considerable number of micromixer concepts has been published in literature, the question of how to operate these mixers in order to obtain optimal mixing results is usually not answered. Very few research deals with this issue including the work of Ansari [29] and Cortes-Quiroz [30] who report on optimized geometries of herringbone mixers. Generally, the control parameters to achieve high mixing performance are rather intuitionally derived. Hence, in the present article we focus on the investigation and optimization of the electrokinetic micromixer introduced in [28]. At first, a short overview of the mixer concept and design is given. We proceed to the next section by introducing our 3D mathematical model of the physicochemical processes within the micromixer based on the method of matched asymptotic expansions. This model is implemented in a numerical code which is used to perform simulations of the flow, concentration and electric potential field. The model and the numerical schemes are verified by comparison with the analogous flow experiments. An extensive discussion of the simulated flow and concentration fields follows. Eventually, the validated simulation code is employed for a numerical optimization of the micromixer in order to achieve high mixing degrees in short operation times. In detail, we optimize the electrokinetic flow by finding the best frequency and amplitude for two forms of electrical excitations, a continuous (sine) and a discrete (square) waveform, and compare the resulting mixing performances. Finally, this article is summarized with some concluding remarks.

II. ELECTROKINETIC MICROMIXER

The micromixer geometry under investigation comprises two inlet channels, forming a Y-junction, and a subsequent single meander geometry located downstream in the common outlet channel. The merging channels of the Y-junction feature an angle of 40°. The

liquids to be mixed flow through the inlet channels and merge at the Y junction. This base flow is pressure-driven and can be created by employing displacement (syringe) pumps, for instance. Without an applied electric potential difference, an even, layered flow is observed in the common channel. Here, mixing of the liquids occurs only by diffusion across the (virtual) contact interface of the layered flows. The mixing performance can be considerably improved by applying an alternating potential difference along the microchannel axis which induces an oscillating electrokinetic flow. The electrokinetic flow creates a secondary velocity component which is, within the bends of the meander channel geometry, perpendicularly-directed to the pressure-driven main flow. This secondary velocity component stretches and folds the contact interface of the liquids resulting in higher mixing degrees at the micromixer outlet.

The micromixer concept has been realized for the sake of experimental characterization as described in our previous works [31, 32]. The channel geometry is microfabricated by a lithography process in a microfluidic chip made out of FOTURAN glass and is built of three layers. The base layer is made of FOTURAN of 1000 μm thickness, with a number of etched holes for inflow and outflow and for accurate relative positioning of the three layers. The mixer layer is made of FOTURAN of 110 μm thickness in which channels of wideness d_0 =110 μm are etched. Consequently, all these flow channels have, to good accuracy, square cross-sections of $110\mu m \times 110\mu m$. Figure 1 gives a schematic drawing of the experimental micromixer setup and mode of operation. The inlet channels and the outlet

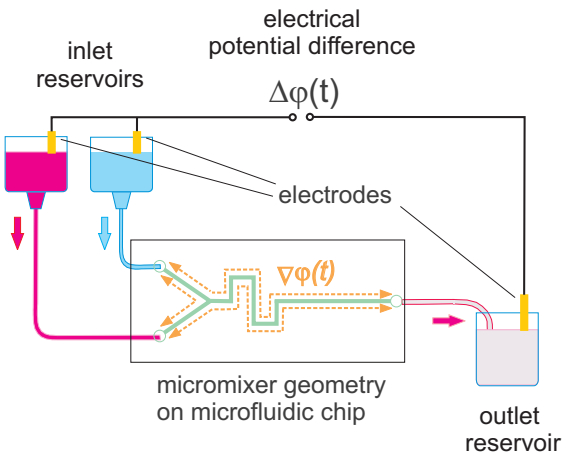

FIG. 1. Sketch of the electrokinetic micromixer principle.

channel are connected with two inlet reservoirs and an outlet reservoir, respectively, enabling a gravity-driven non-pulsating base flow of small Reynolds numbers. A DC power supply in conjunction with a function generator allows to apply time-dependent potential differences $\Delta\varphi(t)$ of desired waveform, amplitude and frequency between the electrodes immersed in the reservoirs. The inlet electrodes are electrically connected so that the potentials in both inlet reservoirs are identical.

III. SIMULATION METHODOLOGY

A. Mathematical formulation of electrical potential, flow and concentration field

In this section, a brief introduction of a mathematical model capable of describing the physicochemical phenomena within the micromixer is given. The model is based on the method of matched asymptotic expansions (cf. [33]); a detailed derivation of the model is published elsewhere [32]. The model comprises the governing equation of the electrical potential φ, flow field $(v, u, w)^T$, pressure p, and the species concentration c_i. The equations are related to a local wall-normal and wall-tangential coordinate system $(x, y, z)^T$ with the origin at the channel wall. In detail, the model consists of the Poisson-Boltzmann equation, the Navier-Stokes equation extended by a Coulomb force term, and a convection-diffusion species transport equation. All equations are non-dimensionalized with a length scale, a convective velocity scale, a viscous pressure scale, a convective time scale, a potential scale, and a concentration scale; we use:

$$\vec{X} = \frac{\vec{x}}{d_0},\ \vec{V} = \frac{\vec{v}}{u_0},\ P = \frac{p d_0}{\mu u_0},\ T = \frac{t}{t_0},\ \Phi = \frac{\varphi}{\Delta\varphi_0},\ C_i = \frac{c_i}{c_0}. \tag{1}$$

Within the scaling (1), d_0 denotes the channel width, u_0 is the average axial velocity in the common channel, $t_0 = d_0/u_0$ is a convective time scale, μ is the dynamic viscosity, $\Delta\varphi_0$ is a typical potential difference (e.g. between inlet and outlet electrodes), and c_0 is the initial species concentration. The non-dimensionalization of the governing equations shows two domains which can be distinguished by whether to or not a Coulomb force acts on the liquid. That is, the electrically-neutral bulk liquid and the electrically-charged electrical double layer (EDL). We find approximate analytical solutions for electrical potential, flow, pressure and concentration fields within the EDL. These solutions are employed, using the

method of matched asymptotic expansions, to infer (transition) boundary conditions for the electrically-neutral bulk liquid which has to be solved numerically. Consequently, a very fine mesh resolution of the EDL, resulting in expensive numerical costs, is omitted.

In detail, in terms of the electrical potential, non-dimensionalization and asymptotic matching lead to a Laplace equation in conjunction with a Neumann boundary condition at the transition between bulk liquid and EDL. That is,

$$\Delta\Phi \simeq 0, \tag{2}$$

$$\frac{\partial\Phi(X,Y,0)}{\partial Z} \simeq 0. \tag{3}$$

Here, we treat the electrical potential as quasi-instantaneous since the time for its establishment is much smaller than the convective time scale of the flow. However, we account for the time-dependency of the electrical potential by introducing a non-dimensionalized excitation frequency corresponding to a Strouhal number

$$St = \frac{f d_0}{u_0} = f t_0 \tag{4}$$

where f is the dimensional frequency of the electrical potential.

For the flow in the bulk liquid, we obtain the governing equations according to

$$\nabla \cdot \vec{V} = 0 \,, \tag{5}$$

$$Re\left(\frac{\partial\vec{V}}{\partial T} + (\vec{V}\cdot\nabla)\vec{V}\right) = -\nabla P + \Delta\vec{V} \,, \tag{6}$$

with the corresponding boundary conditions:

$$U(T,X,Y,0) \simeq -\Pi\frac{\partial\Phi}{\partial X} \,, \tag{7}$$

$$V(T,X,Y,0) \simeq -\Pi\frac{\partial\Phi}{\partial Y} \,, \tag{8}$$

$$W(T,X,Y,0) \simeq 0 \,, \tag{9}$$

$$P(T,X,Y,0) \simeq C(T,X,Y) \,. \tag{10}$$

Two dimensionless groups arise from non-dimensionalization; the Reynolds number $Re = u_0 d_0/\nu$ and $\Pi = \dfrac{l_D q_\zeta \Delta\varphi_0}{u_0 d_0 \mu}$ which can be interpreted as the ratio of electric to viscous forces. Here, ν denotes the kinematic viscosity of the liquid, l_D is the Debye length, and q_ζ is the charge density at the shear layer of the EDL. We see that any wall-tangential electrical potential difference (gradient) leads to a finite velocity transition condition for the bulk

solution. The boundary velocity conditions (7,8) correspond to the well-known Helmholtz-Smoluchowski slip velocity (cf. [34]). However, there is a distinct difference between both approaches. Smoluchowski essentially neglected the thickness of the EDL and introduced the effect of the EDL by means of the slip velocity while the velocity decrease to zero at the channel wall is not captured. In our approach, the slip velocity appears naturally at the transition between bulk and EDL solution. Hence, the overall solution, which is based on superposition of bulk and asymptotic EDL solutions, captures the velocity decrease and fulfills the no-slip condition at the wall.

The concentration field of species i is simulated by means of a standard convection-diffusion equation. We arrive after non-dimensionalization in the following governing equation and boundary conditions:

$$\frac{\partial C_i}{\partial T} + \nabla \cdot (\vec{V} C_i) = \frac{1}{ReSc_i} \Delta C_i \ , \tag{11}$$

$$\frac{\partial C_i(X, Y, 0)}{\partial Z} = 0 \ . \tag{12}$$

Here, $Sc_i = \nu / D_i$ is the Schmidt number of species i which is a measure for the ratio of convective to diffusive species transfer rate.

B. Computational Procedure

The mathematical model, discussed in the previous section, is implemented in an in-house code HiFlow^3 (www.hiflow3.org) developed by the Engineering Mathematics and Computing Lab (EMCL) at Karlsruhe Institute of Technology (KIT). HiFlow^3 is a multi-purpose Finite-Element-Method toolbox capable for solution of a wide range of physical problems modeled by partial differential equations. Parallel Computing – as the foundation for high performance simulations on modern computing systems - is introduced on two levels: (i) Coarse-grained parallelism by means of distributed grids and distributed data structures; (ii) fine-grained parallelism by means of platform-optimized linear algebra back-ends. Modern numerical schemes in HiFlow^3 are built on top of both levels of parallelism; further information is available in [35]. In the present work, two different high-performance computers are used for the simulations. The first set of micromixer simulations is performed on the distributed memory parallel computer HP XC3000 at Steinbuch Centre for Computing, KIT, Germany equipped with 288 computation nodes. Each node contains two

Quad-core Intel Xeon X5540 (2.53 GHz) CPUs and 24 GB of main memory. For the numerical micromixer optimization, we employ the high-performance computer JUROPA-JSC at Forschungszentrum Jülich, Germany equipped with 2208 nodes. Each node is equipped with two Quad-core Intel Xeon X5570 CPUs (2.93 GHz) and 24 GB of main memory.

Despite of these impressive computational resources, we have to limit the computational domain to the meander as shown in figure 2 in order to obtain reasonable computation times. This computational domain is "cut out" of the complete micromixer geometry in a

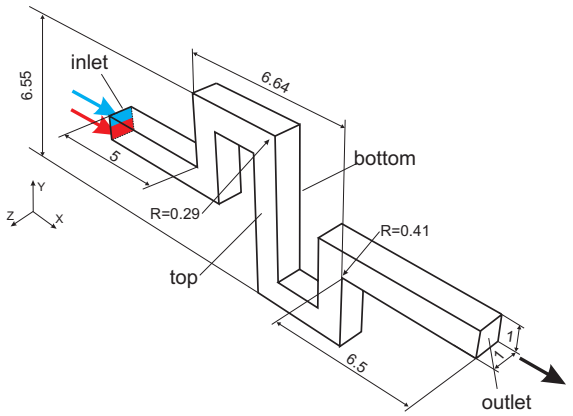

FIG. 2. Sketch of the computational domain (without rounded corners).

distance of five channel widths upstream of the first bend and six and a half channel widths downstream of the last bend, respectively. Note that all dimensions in figure 2 are scaled by the channel width $d_0 = 110\mu m$. Due to the fabrication process, we find two different types of corners in the mixer geometry. The radii of the inside and outside corners are $0.41\,(4.5\mu m)$ and $0.29\,(3.2\mu m)$, respectively. As the entire microchannel consists of three glass layers, the junction of top and bottom walls to side walls is idealized by right angles. At all boundaries of the computational domain, adequate boundary conditions have to be formulated reflecting the corresponding physics of the complete set-up. According to our mathematical model, the "channel walls" indicate the transition between liquid bulk and EDL.

The model liquids to be mixed are pure water and water with a dissolved tracer. We assume that the tracer does not change the properties of the water so that all liquid parameters are identical. Density and dynamic viscosity of the liquid are $\rho = 1000kg/m^3$ and

$10^{-3}Pas$, respectively. The diffusion coefficient of the tracer is $D = 4.27 \cdot 10^{-10}m^2/s$ which consequently arrives in a Schmidt number of $Sc = 2340$. We have to define reasonable initial and boundary conditions for the concentration field which is not a trivial task. The upstream Y-junction where both liquids meet is not part of the computational domain. We decide to use a rather artificial initial concentration field. At the lower half of the inlet cross-section, we implement a concentration of $C = 1$, while at the upper half $C = 0$ is used. Accordingly, the entire lower and upper half of the microchannels have an initial ($T = 0$) concentration of $C = 1$ and $C = 0$, respectively. A vanishing flux condition $\partial C/\partial Z = 0$ is engaged at the micromixer outlet and at all transition layers liquid bulk–EDL. To infer appropriate boundary conditions for the electrical potential, we estimate that 4.7% of the potential difference $\Delta\varphi$ between inlet and outlet reservoir electrodes drops over the computational domain. Our experiments have typically been performed using potential differences of about 1kV so that we choose $\Delta\varphi_0 = 47V$ as an appropriate scaling parameter for the electrical potential. In principle, the boundary conditions for the potential at the inlet and outlet alternate in time between $\Phi_{in} \sim 1, \Phi_{out} = 0$ and $\Phi_{in} = 0, \Phi_{out} \sim 1$. For the sake of simplification, we permanently set the inlet potential in the computations to be zero and consider only the corresponding outlet potential from now on. At the transition between the liquid bulk solution and the EDL solution $\partial\Phi/\partial Z = 0$ is enforced.

To realize the pressure-driven base flow, we implement a tangential body force within the first straight channel part in conjunction with fully-developed flow conditions, i.e. $\partial U/\partial X = V = W = 0$) at the inlet and outlet cross-section (Here, X and U are directed downstream along the channel axis). The value of the body force is adjusted to establish the desired Reynolds number in the common channel. Throughout all computations, the velocity and time scales are $u_0 = 9.1 \cdot 10^{-4}m/s$ and $t_0 = 0.121s$, respectively. The electrokinetic flow is introduced into the liquid bulk solution via boundary conditions (7,8). Previous experiments have revealed that the charge density at the microchannel wall and the Debye length correspond to $q_\zeta = 2.2 \cdot 10^{-3}C/m^2$ and $l_D \simeq 216nm$ [32]. Hence, we calculate the ratio of electrical to viscous forces to be $\Pi = 21.36$ which is used throughout the simulations.

IV. FLOW AND CONCENTRATION FIELD

A. Flow Field

Each mathematical model and its numerical implementation has to be validated to make it a suitable tool for optimization purposes. In this section, we compare three-dimensional (3D) numerical simulations to our experimental results obtained with Micro Particle Image Velocimetry (μPIV) as described in [32]. In detail, we focus on selected flow fields which can be found within the lower bends of the micromixer. The Reynolds number of the pressure-driven flow is $Re = 0.1$. The electrokinetic flow is excited by an alternating potential difference of $\Delta\varphi = 1000V$ between the electrodes featuring a square waveform and a frequency of $f = 0.1Hz$. Scaling results in according Strouhal number and outlet potential amplitude of $St = 0.012$ and $\widehat{\Phi}_{out} = 1$, respectively. We observe two different flow regimes within the micromixer depending on the polarity of the electrical potential difference. These flow regimes are, of course, time-dependent. However, within almost the entire half of a wave period, the flow can be considered as (quasi-)steady since the transition between the flow regimes occurs very quickly. For an outlet potential of $\Phi_{out} = 1$, the induced electrokinetic flow is equally directed to the pressure-driven base flow; an even and quasi-steady flow is observed (not shown graphically). The flow regime changes drastically when the electrode polarity changes, i.e. $\Phi_{out} = -1$. The electrokinetic flow is now directed upstream, i.e. against the pressure-driven base flow. This counterflow situation in conjunction with the meander geometry gives rise to highly interesting flow fields which considerably support mixing. Figure 3 shows selected flow fields by means of particle paths, i.e. we integrate the movement of particles due to the velocity field in planes of constant heights. This method allows us to infer the flow topology in terms of singular, i.e. vortex and saddle, points, and results in a demonstrative illustration of the complex flow regime. The upper row of figure 3 shows the flow topology measured by μPIV while the lower row displays the results of our numerical simulations.

Figure 3(a) depicts the flow topology at a height level of $Z = -0.43$. The measured and simulated pathlines indicate a (quasi-steady) flow from right to left through the meander segment. At this height level close to the bottom wall at $Z = -0.5$, the flow field is dominated by the electrokinetic flow.

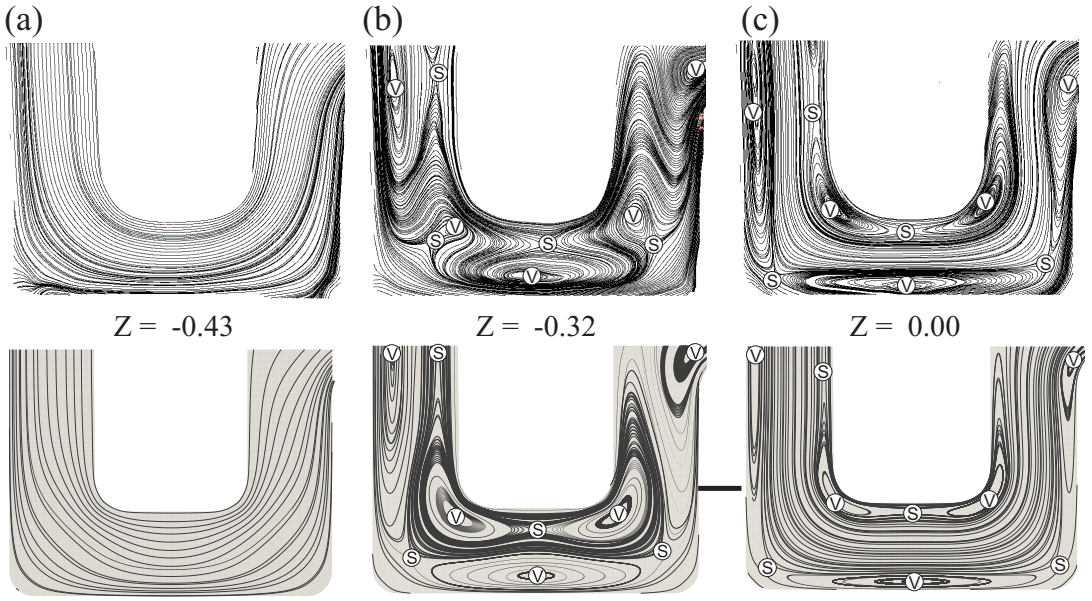

FIG. 3. Measured (upper row) and simulated (lower row) pathlines of the flow at height levels (a) Z=-0.43, (b) Z=-0.32 and (c) Z=0.00. The flow consists of a pressure-driven base flow with Re=0.1 and a counter-directed electrokinetic flow.

If we move towards the midplane of the meander segment, the topology of the flow field changes drastically as indicated in figure 3(b) which shows pathlines at a height level of $Z = -0.32$. The measured pathlines are strongly stretched and folded resulting in a complex flow topology which features various singular points. We find a vortex point (v) and a saddle point (s) in the left (vertical) channel segment, whereas in the right (vertical) channel segment, only a vortex point is found. Another set of vortex and saddle points is observed in the middle (horizontal) channel segment. Furthermore, we find a pair of saddle and vortex points within each bend. This complex flow field results from the mutual influence of the electrokinetic and pressure-driven flows present close to all channel walls and within the channel core, respectively. If we compare measured and simulated pathlines, the overall picture is in a very good agreement. All singular points are rediscovered featuring an equal type and almost identical positions. Likewise, the characteristics of the pathlines appear similar within the channel segment.

The flow topology in the mid-height level ($Z = 0$) of the meander segment is presented in figure 3(c). The measured pathlines reveal a quasi-steady and even flow, from left to right,

which is the pressure-driven part of the flow located within the centre of the microchannel. Adjacent to the walls, the electrokinetic part of the flow is counter-directed from right to left giving rise to several singular points located at the (shear) interface between the two flows. In detail, we rediscover all singular points known from height level $Z = -0.32$, whereas some positions are slightly changed. For instance, saddle and vortex points previously located in the bend centers are moved towards the bend corners. The comparison between measured and simulated pathlines shows again a very good agreement with respect to type and position of the singular points and the pathlines characteristics.

The present results reveal some further interesting aspects when we refer to our previous work [32] where we compared measured and simulated pathlines obtained with a different numerical code and, more importantly, with a simplified numerical mesh structure. The simplified mesh consisted of a perfect rectangular geometry featuring sharp edges and corners which cannot be achieved in reality due to constraints imposed by microfabrication processes, e.g. by etching. The overall comparison revealed a good agreement as well but there was a distinct topology difference within the inner (protruding) corner of the bends. We previously obtained two vortices and a separating saddle in the simulations. In contrast, the present study shows a single vortex and a separating saddle in both experimental and simulation results. We concluded that the difference is due to the sharp edges/corners; an assumption which is verified by the simulations in this work performed with a mesh corresponding to a more realistic micromixer geometry.

To summarize, the comparison of measured and simulated results proves that the numerical code HiFlow^3 is able to reproduce the complex flow fields in the electrokinetic micromixer with an excellent agreement. This validation of the mathematical models and their numerical implementations with respect to the flow field serves as a basis for further simulations of the concentration fields and, eventually, for the electrokinetic optimization.

B. Concentration Field

We now focus on different concentration fields which are present in the micromixer as a result of different (non-optimized) electrical excitations. We only present results of numerical

simulations since the measurement of complex, time-dependent 3D concentration fields in microchannels is a rather difficult task. In our previous work [31], a Micro Laser-Induced Fluorescence (μLIF) has been engaged to investigate the influence of Dean vortices, induced by a pure pressure-driven flow, on the concentration field within the micromixer geometry. In contrast to the application of fluorescence intensity techniques to macroscopic flows (LIF), this method illuminates the complete microchannel volume. This results in height-averaged concentration fields which can be easily misinterpreted. In principle, if a LIF method is coupled with a scanning confocal microscope, as shown in [36] for mixing in slug flows, measurements of 3D concentration fields in microstructures are possible. However, even for microchannels, the scanning across the channel height takes a relatively long time. Thus, this method is restricted to steady concentration fields or to concentration fields with a regular recurrence of patterns so that the measurements can be synchronized.

Figure 4 shows the concentration field within the midplane of the micromixer for different modes of electrical excitation. The Reynolds and Schmidt numbers are $Re = 1$ and $Sc = 2340$, respectively, and the simulation time is $T = 30$. Figure 4(a) shows the concentration field for a pure pressure-driven flow without any electrical excitation corresponding to a Strouhal Number of $St = 0$. We basically recognize three layers of liquid. The lower (red) layer is at tracer concentrations around $C = 1$ and the upper (blue) layer is at concentrations around $C = 0$. Further, a thin (green) concentration boundary layer of mixed liquid ($C = 0.5$) is present between the upper and the lower layer. In the absence of electrical excitation, it can be clearly seen that mixing occurs only by diffusion across the contact interface of both (blue and red) liquids. The thickness of this concentration boundary layer increases along the channel axis as the residence time of the liquids increases.

Figure 4(b) shows the concentration field as a result of a constant electrical potential $\Phi_{out} = 1$ which can be interpreted as a wave of infinite high frequency, i.e. $St \mapsto \infty$. The electrical potential induces an electrokinetic flow which is counter-directed to the pressure-driven base flow. Comparable to figure 4(a), we find an even concentration field characterized by three liquid layers. In contrast to figure 4(a), however, it can be seen that the concentration boundary layer between blue and red liquid is wider. This implies that a higher fraction of mixed liquid leaves the mixer outlet compared to the pure pressure-driven flow regime. This can be simply explained by the residence time. The counter-directed electrokinetic flow decreases the total flow rate. Hence, the residence time of the liquids within the

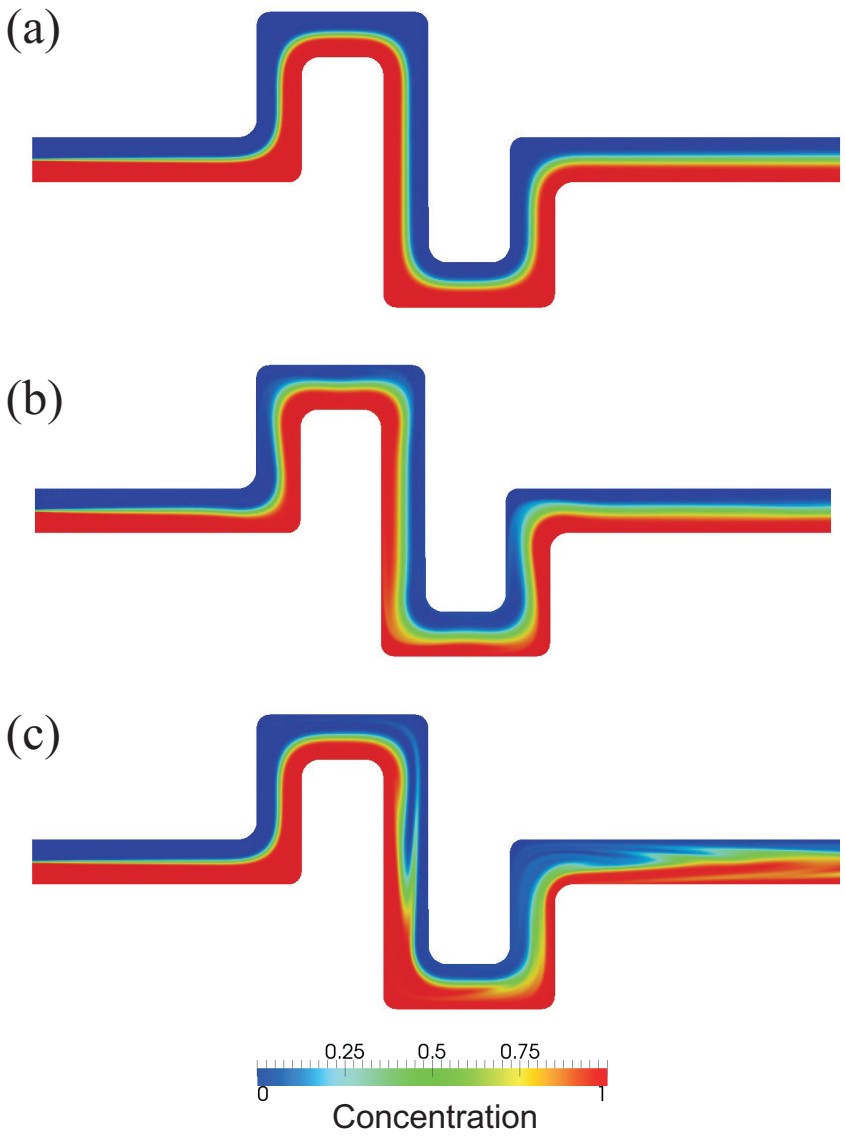

FIG. 4. 3D Simulations of the concentration field within the midplane of the micromixer at $T = 30$ for different modes of electrical excitations: (a) pure pressure-driven flow; (b) pressure-driven flow with a steady counter-directed electrokinetic flow; and (c) pressure-driven flow and an alternating electrokinetic flow. The Reynolds and Schmidt numbers are $Re = 1$ and $Sc = 2340$, respectively.

mixer geometry is increased and there is more time for diffusive mixing across the contact interface.

The concentration field for the micromixer operated with a time-dependent electrical

excitation is given by figure 4(c). Here, the outlet electrical potential has a square waveform, an amplitude of between $\widehat{\Phi}_{out} = 1$ and alternates with a frequency corresponding to $St = 0.012$. We find locations where the concentration boundary layer is folded and stretched which increases the contact interface area and, consequently, facilitates mixing by diffusion. The stretching and folding is induced by the interaction of the meandering geometry and the alternating electrokinetic flow. The electrokinetic flow is perpendicular-directed to the pressure-driven base flow within the bends. This secondary flow transports liquid by convection across the channel center into locations previously occupied by the other liquid. Additionally, the flow regime switches between an even flow and the flow fields illustrated in figure 3. The complex flow topologies close to the channel walls as a result of mutual influence of pressure-driven and (counter-directed) electrokinetic flow contribute to mixing as well. Even though the performance might be better than for the previous operation modes, it is obvious that the mixer does not operate at its best. The electrical excitation settings used here are inferred from the μPIV experiments described in section IV A, and cannot necessarily be employed to achieve good mixing. Eventually, all shown concentration fields demonstrate the need for an optimization of the micromixer's mode of operation.

V. OPTIMIZATION

In this section, we employ the validated numerical tools to optimize the mixing performance of the electrokinetic micromixer. Even though we have access to considerable computational resources, in terms of optimization we have to further restrict simulations. The dimensionless tracer diffusion coefficient of our mixing problem ($Re = 1$, $Sc = 2340$) is given as $D = 1/(ReSc)$. This value in conjunction with the cell Peclet number $Pe_c = UL/D$ allows to infer a roughly-suitable mesh size L for our computations. Given a mean velocity of $U \simeq 1$ and the necessary condition that $Pe \lesssim 1$, the maximal size of a mesh cell should be $L \lesssim 1/2340 \approx 0.0004\,(0.05\mu m)$. A 3D optimization with such a fine mesh is far beyond the computational capabilities accessible for this work. Hence, we concentrate on 2D optimizations and restrict the computations to the midplane (Z=0) of the micromixer. This simplification is justified after inspecting the concentration fields of the micromixer at different height levels (not shown). Even though the flow topology changes considerably along the channel height (cf. figure 3), the concentration fields are similar. Likewise, a

comparison of midplane flow and concentration fields obtained from 3D and 2D simulations reveals a very good qualitative agreement; see [37] for details.

In general, we have to identify the common features of a optimization problem prior to the application optimization techniques [38]. That is: (i) A quantitative criterion that has to be optimized which is usually formulated as a cost functional; (ii) One or more control or design parameters that can be modified to achieve an optimization; (iii) And finally, the constraints which have to be fulfilled within the optimization problem.

A simple approach to express perfect mixing of two liquids is to correlate it to a respective concentration C_M. In the case of two identical liquids with ($C = 1$) and without tracer ($C = 0$), perfect mixing is given for a concentration of $C_M = 0.5$. A practical, quantitative mixing criterion can be achieved by integrating the quadratic difference from perfect mixing in an area of interest Ω_s for each time step. Hence, the cost functional for the optimization is defined to be

$$J(C,T) \equiv \int_{\Omega_s} (C(T) - C_M)^2 d\vec{X}. \tag{13}$$

We consider the last horizontal channel segment of the meander as the area of interest Ω_s. Eventually, perfect mixing is achieved when the cost functional $J(C,T)$ is zero.

The performance of the micromixer can be effectively influenced by different control/design parameters. These include geometric factors, such as number of bends or length ratio of horizontal to vertical channel segments, and flow parameters, such as the Reynolds number, which can be adjusted more easily. In this work, we restrict the optimization efforts to the secondary electrokinetic flow which can be conveniently manipulated in form of the electrical excitation (control) parameters α_k including outlet potential's amplitude $\widehat{\Phi}$, frequency (Strouhal number St) and waveform. In detail, we perform optimizations for two different outlet potentials featuring a discrete and a continuous waveform. The first optimization is performed using a discrete square wave potential. We choose a Fourier series approximation for the sake of differentiability, i.e.

$$\Phi_{out,1}(T,\alpha_k) = \frac{4\widehat{\Phi}_1}{\pi} \sum_{j=0}^{n} \frac{\sin((2j-1)2\pi St_1 T)}{2j-1}. \tag{14}$$

Practically, we limit the number of Fourier terms to n=10. The second optimization is

performed for a continuous outlet potential of sinusoidal waveform. That is:

$$\Phi_{out,2}(T, \alpha_k) = \Phi_2 + \widehat{\Phi}_2 \sin(2\pi St_2 T) \tag{15}$$

with the potential offset Φ_2 as additional control parameter. The constraints within our optimization problem are specified by the mathematical model and the corresponding boundary conditions as described in section III. In terms of practical applications, rapid mixing is also a desirable feature and we therefore restrict the time interval to be $T \in [0, 30]$.

Common optimization methods can principally be distinguished by the determination of the cost functional gradient. Two approaches are common, the adjoint- and the sensitivity-based approach. Both approaches calculate the gradient of the cost functional with respect to the control parameter to solve the optimization problem. For a time dependent problem, the adjoint-based approach requires forward- and backward-in-time solutions of the adjoint equations while sensitivity-based methods only project forward in time. That is, the adjoint-based approach determines $\nabla J(C, \alpha_k)$ simultaneously and independent of the number of parameters α_k , whereas the sensitivity-based approach requires the solution of a linearized problem for each α_k. In this work, we use a sensitivity-based approach, whereas the chain rule is applied to derive the gradient of the cost functional (13). Eventually, the optimization problem of the electrokinetic micromixer can be formulated as

$$\min_{C,\alpha_k} J(C, \alpha_k) \equiv \frac{1}{2} \int_0^T \int_{\Omega_s} (C(T) - C_M)^2 d\vec{X} dT + \frac{\lambda}{2} \sum_{k=1}^{m} |\alpha_k^2|, \tag{16}$$

whereas λ is the regularization term which can be chosen to control the optimization problem and m is the number of control parameters of the optimization problem. Further information on the sensitivity-based optimization methods used in our work can be found in [38–41].

We solve the optimization problem for a flow of $Re = 1$ and two different electrical excitations $\Phi_{out,1}$,$\Phi_{out,2}$ so that the mathematical model, boundary conditions and equation (16) are fulfilled. The resulting optimized control parameters for both waveforms are given in Table I. The optimization of the discrete (square waveform) outlet potential $\Phi_{out,1}$ indicates best mixing for an amplitude and frequency of $\widehat{\Phi}_1 = 1.490$ and $St_1 = 0.208$, respectively.

Excitation	Offset	Amplitude	Frequency
square wave potential $\Phi_{out,1}$	–	$\widehat{\Phi}_1 = 1.490$	$St_1 = 0.208$
sine wave potential $\Phi_{out,2}$	$\Phi_2 = 0.018$	$\widehat{\Phi}_2 = 1.476$	$St_2 = 0.210$

TABLE I. Optimized control parameters for two different electrical excitations.

Regarding the continuous (sine waveform) electrical excitation, the optimization shows no need for an offset of the potential. The optimal amplitude and frequency are $\widehat{\Phi}_2 = 1.476$ and $St = 0.210$, respectively. Surprisingly, there is no distinct difference between the continuous and the discrete electrical excitation parameters but the waveform. To obtain a better insight into the mixing performance, we plot the evolution of the cost functional (degree of mixing) vs. the simulation time for different electrical excitation modes in figure 5.

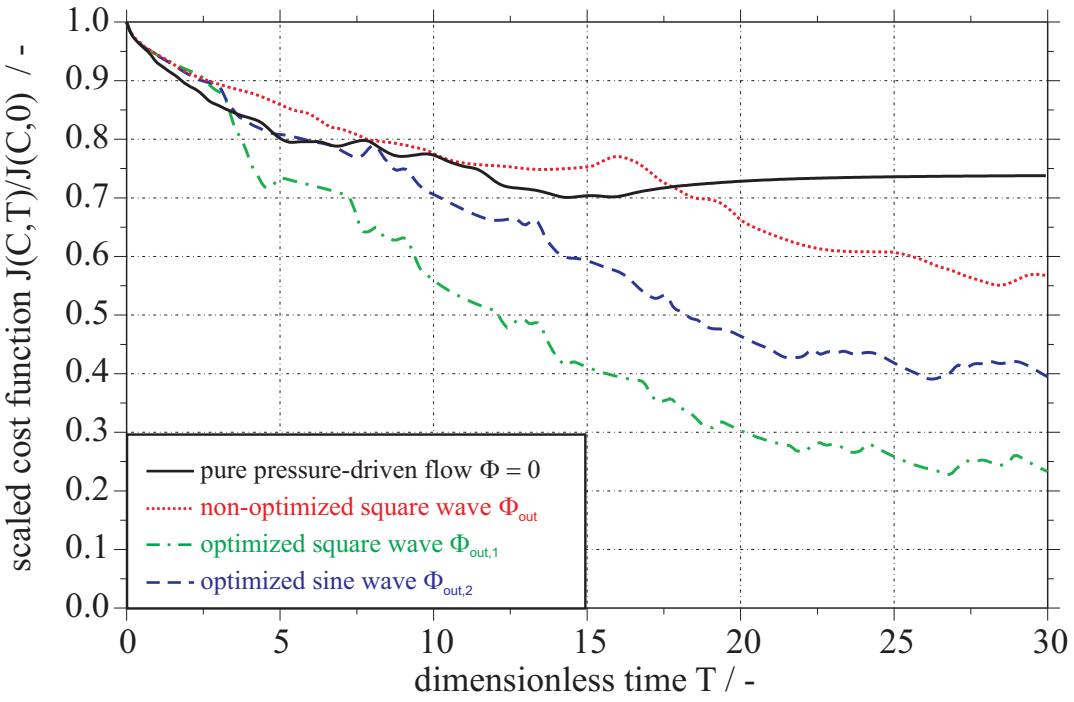

FIG. 5. Evolution of the cost functional, scaled with the (initial) value at T=0, vs. the dimensionless simulation time T for different modes of electrical excitation.

In detail, we plot the cost functional $J(C,T)$, scaled with the (initial) cost functional at $T = 0$ for the pure pressure-driven flow, for the non-optimized square wave potential as

discussed in section IV B, and for the optimized square and sine waveform potentials. The pure pressure-driven flow (solid line) without any electrical excitation indicates the baseline for all cases. We see that starting from a value of 1, the scaled cost functional decreases to about 0.7 at $T \approx 15$ and then slowly approaches a steady value of about 0.73 resulting from the (artificial) initial conditions of two totally unmixed liquids that we employ in all simulations. The steady value is related to the concentration boundary layer between the two layered liquids and is the minimum degree of mixing which can be achieved for the given mixing configuration. Additionally, this plot allows to infer the mean residence time of the mixer at the given mode of operation. The initial concentration condition can be interpreted as a perturbation of the steady-state concentration field. The time to sweep out the perturbation from the micromixer domain, i.e. the mean residence time, is displayed by the time required to achieve a steady cost functional, i.e. $T_m \simeq 20\,(t_m \simeq 2.4s)$.

The mixer operated with the non-optimized square wave potential $\Phi_{out}(\widehat{\Phi} = 1, St = 0.012)$ (dotted line) achieves a value of about 0.56 at $T = 30$. This represents a performance improvement compared to the mixer with the pure pressure-driven flow even though the electrical excitation setting was chosen arbitrarily. When the micromixer is operated with the optimized potentials, higher mixing degrees in shorter mixing times are generally achieved compared to the previous cases. The mixer excited with the sine wave potential $\Phi_{out,2}$ (dashed line) approaches a final value of 0.4, whereas the operation with the square wave potential $\Phi_{out,1}$ (dash-dot line) results in 0.26 at $T = 30$. Eventually, even though amplitude and frequency of both optimized potentials are similar, the performance of the mixer operated with the discrete signal is distinctively superior to the mixer operated with the continuous signal.

Figure 6 shows the optimized concentration fields in the micromixer at the end of the optimization interval ($T = 30$), which gives an illustrative demonstration of the cost functionals. In detail, figure 6(a) illustrates the situation when the electrokinetic flow is excited by the optimized sine wave potential $\Phi_{out,2}$. The concentration boundary layer is strongly distorted and we find locations where one liquid is (almost) entirely enclosed by the other. Nevertheless, even though a considerable fraction of Ω_s is occupied by mixed liquid, the concentration field is somewhat heterogenous. When the mixer is operated with the optimized square wave potential $\Phi_{out,1}$, we find improved mixing results as already indicated by the lowest scaled cost functional. The domain Ω_s is mainly filled with mixed liquid, whereas

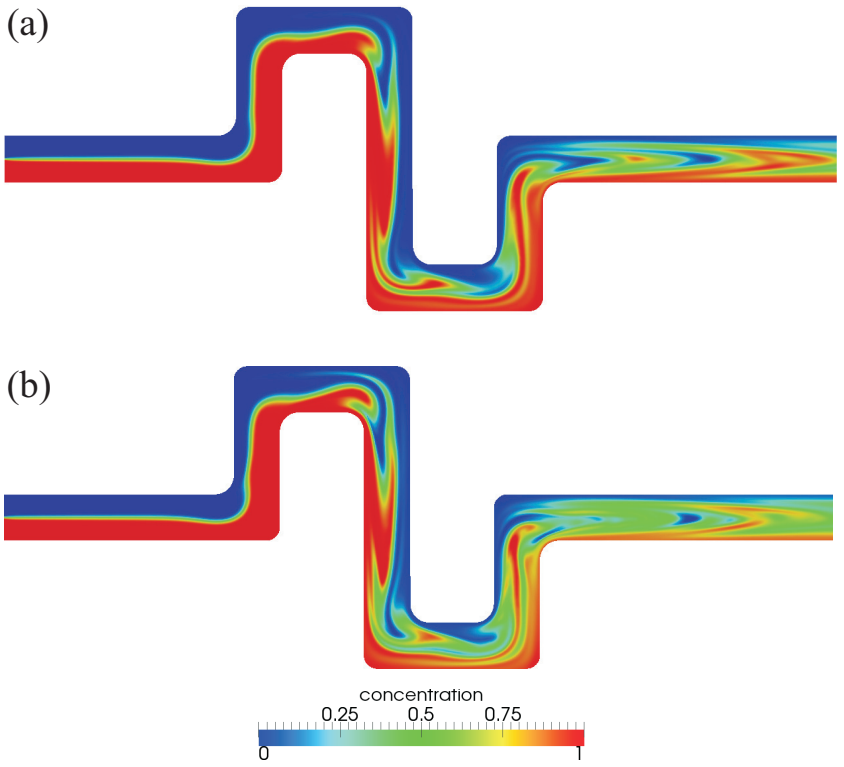

FIG. 6. Concentration fields in the midplane of the micromixer at $T = 30$. The flow consists of a pressure-driven base flow with $Re = 1$ and an optimized electrokinetic flow induced by (a) sine and (b) square wave potential.

some minor unmixed areas are present as well. Again, the difference in the electrical excitation resulting in the optimized concentration fields plotted in figure 6(a) and (b), is just the waveform. Interestingly, when we compare the concentration fields, we find in principle similar patterns. That is, the track of the concentration boundary layer(s) is comparable for both excitations; obviously a result of the similar amplitudes and frequencies. However, it appears, especially in the first half of the mixer geometry, that the discrete potential results in a more pronounced stretching and folding. This is presumably related to the duration of the velocity amplitude of the secondary flow. The square wave potential induces a maximum electrokinetic velocity which is present over almost the entire half of the wave period. The electrokinetic velocity as a result of the sine wave potential, however, increases continuously from zero to the maximum value over one quarter of the period and immediately decreases again. Consequently, there is less convective transport of liquid across the channel center

towards the other liquid when operated with the continuous signal.

VI. CONCLUDING REMARKS

In this article, we undertake investigations on the optimization of an electrokinetic micromixer. The conceptual approach of the micromixer is realized by inducing a secondary (alternating) electrokinetic flow which is partially directed perpendicular to the pressure-driven main flow due to the mixer's meandering geometry. The electrokinetic flow is induced by an alternating electric potential difference applied between the mixer's in- and outlet. Good mixing results can be achieved by using an appropriate ratio of secondary electrokinetic velocity to pressure-driven main flow velocity in conjunction with a respective excitation frequency to obtain folding and stretching of the contact interface of the liquids to be mixed. Suitable modes of electrical excitation, i.e. amplitude, frequency and waveform of the applied potential difference, are not known and respective technical/design guidelines do not exist.

We therefore implement a mathematical model of the electrical potential, flow and concentration field into a Finite-Element-Method code. Model and numerical implementations are validated against experimental observations of the complex flow topology present in the lower channel segment of the micromixer geometry. The comparison of numerical and experimental results shows excellent agreement. The computed concentration fields clarify that, even though an increased mixing performance is observed when the mixer is electrically-excited, the mixer does not operate at its best. Hence, there is a need to optimize the mode of operation which can be done by engaging our validated numerical model in conjunction with adequate numerical optimization strategies.

We restrict the optimization efforts to the electrokinetic flow which can be conveniently controlled in form of the electrical excitation parameters potential amplitude, frequency (Strouhal number) and waveform. Two exemplary waveforms are chosen, a square wave and a sine wave potential representing a discrete and a continuous excitation. It turns out that the optimized amplitudes and frequency for both electrical excitation modes are almost identical. Here, the optimized outlet electrical potentials induce a (secondary) electrokinetic flow amplitude which is about 10% of the pressure-driven main flow amplitude. The optimized frequencies correspond to approximately 1/5 of the inverse convective time scale t_0^{-1}.

The most noteworthy observation of the present optimization results is the influence of the waveform. A considerable superior mixing performance is observed for the discrete over the continuous excitation, even though amplitudes and frequencies are similar.

In summary, the present work demonstrates that the electrokinetic mixing concept is able to achieve high mixing degrees in short operation times, given a reasonable ratio of main flow to secondary flow amplitudes and an appropriate excitation frequency. The question whether to or not other electrical excitation waveforms, discrete or continuous, exist which result in improved mixing degrees at shorter times must be answered in future work. Eventually, an optimization with a completely arbitrary electrical potential, using the adjoint-based optimization approach, is desirable but this would require very expensive computations.

---

[1] H.A. Stone, A.D. Stroock, and A. Ajdari, "Engineering flows in small devices: Microfluidics toward a lab-on-a-chip," Annu. Rev. Fluid Mech. **36**, 381–411 (2004)

[2] T.M. Squires and S.R. Quake, "Microfluidics: Fluid physics at the nanoliter scale," Rev. Mod. Phys. **77**, 977–1026 (2005)

[3] P. Nghe, E. Terriac, M. Schneider, Z.Z. Li, M. Cloitre, and P. Abecassisa, B. Tabeling, "Microfluidics and complex fluids," Lab Chip **11**, 788–794 (2011)

[4] E. Kamio, T. Ono, and H. Yoshizawa, "Design of a new static micromixer having simple structure and excellent mixing performance," Lab Chip **9**, 1809–1812 (2009)

[5] Y.-C. Lin, Y.-C. Chung, and C.-Y. Wu, "Mixing enhancement of the passive microfluidic mixer with j-shaped baffles in the tee channel," Biomed. Microdevices **9**, 215–221 (2007)

[6] Y. Yamaguchi, F. Takagi, K. Yamashita, Nakamura H., H. Maeda, K. Sotowa, K. Kusakabe, Y. Yamasaki, and S. Morooska, "3-d simulation and visualization of laminar flow in a microchannel with hair-pin curves," AIChE J. **50**, 1530–1535 (2004)

[7] C-C. Hong, J.W. Choi, and Ahn C.H., "A novel in-plane passive microfluidic mixer with modified tesla structures," Lab Chip **4**, 109–113 (2004)

[8] J. Melin, G. Giménez, N. Roxhed, W. van der Wijngaart, and Göran Stemme, "A fast passive and planar liquid sample micromixer," Lab Chip **4**, 214–219 (2004)

[9] A.D. Stroock, S.K.W. Dertinger, A. Ajdari, I. Mezić, H.A. Stone, and G.M. Whitesides, "Chaotic mixer for microchannels," Science **295**, 647–651 (2002)

[10] R.H. Liu, A. Stremler, K.V. Sharp, M.G. Olson, J.G. Santiago, R.J. Adrian, H. Aref, and D.J. Beebe, "Passive mixing in a three-dimensional serpentine microchannel," J. Microelectromech. Syst. **9**, 190–197 (2000)

[11] F. Schönfeld, V. Hessel, and C. Hofmann, "An optimised split-and-recombine micro-mixer with uniform "chaotic" mixing," Lab Chip **4**, 65–69 (2004)

[12] Y.-F. Fan and I. Hassan, "Experimental and numerical investigation of a scaled-up passive micromixer using fluorescence technique," Exp. Fluids **49**, 733–747 (2010)

[13] D. Ahmed, X. Mao, J. Shi, B.K. Juluria, and TJ Huang, "A millisecond micromixer via single-bubble-based acoustic streaming," Lab Chip **9**, 2738–2741 (2009)

[14] P.D. Khatavkar, V.V.and Anderson, J.M.J den Toonder, and H.E.H. Meijer, "Active micromixer based on artificial cilia," Phys. Fluids **19**, 083605–1–083605–1 (2007)

[15] M. Yi, S. Qian, and H.H. Bau, "A magnetohydrodynamic chaotic stirrer," J. Fluid Mech. **468**, 153–177 (2002)

[16] S. Oberti, A. Neild, and T.W. Ng, "Microfluidic mixing under low frequency vibration," Lab Chip **9**, 1435–1438 (2009)

[17] D.J. Laser and J.G. Santiago, "A review of micropumps," J. Micromech. Microeng. **14**, R35–R64 (2004)

[18] X. Wang, C. Cheng, S. Wang, and S. Liu, "Electro osmotic pumps and their applications in microfluidic systems," Microfluid Nanofluid **6**, 145–162 (2009)

[19] D.P.J. Barz and P. Ehrhard, "Model and verification of electrokinetic flow and transport in a micro electrophoresis device," Lab Chip **5**, 949–958 (2005)

[20] J. Voldman, "Electrical forces for microscale cell manipulation," Annu. Rev. Biomed. Eng. **8**, 425–454 (2006)

[21] Y. Kang and D. Li, "Electrokinetic motion of particles and cells in microchannels," Microfluid Nanofluid **6**, 431–460 (2009)

[22] A.V. Delgado, F. Gonzalez-Caballero, R.J. Hunter, L.K. Koopal, and J. Lyklema, "Measurement and interpretation of electrokinetic phenomena," J. Colloid Interface Sci. **309**, 194–224 (2007)

[23] M.H. Oddy, J.G. Santiago, and J.C. Mikkelsen, "Electrokinetic instability micromixing," Anal. Chem. **73**, 5822–5832 (2001)

[24] C.-C. Chen, H. Lin, S.K. Lele, and J.G. Santiago, "Convective and absolute electrokinetic

instability with conductivity gradients," J. Fluid Mech. **524**, 263–303 (2005)

[25] A. Ould El Moctar, N. Aubry, and J. Batton, "Electrohydrodynamic microfluidic mixer." Lab Chip **3**, 273–280 (2003)

[26] D. Erickson and D. Li, "Microchannel flow with patchwise and periodic surface heterogeneity," Langmuir **18**, 8949–8959 (2002)

[27] S. Qian and H.H. Bau, "A chaotic electroosmotic stirrer," Anal. Chem. **74**, 3616–3625 (2002)

[28] I. Meisel and P. Ehrhard, "Electrically-excited (electroosmotic) flows in microchannels for mixing applications," Eur. J. Mech. B/Fluids **25**, 491–504 (2006)

[29] M.A. Ansari and K.-Y. Kim, "Shape optimization of a micromixer with staggered herringbone groove," Chem. Eng. Sci. **62**, 6687–6695 (2007)

[30] C.A. Cortes-Quiroz, M. Zangeneh, and A. Goto, "On multi-objective optimization of geometry of staggered herringbone micromixer," Microfluid Nanofluid **7**, 29–43 (2009)

[31] D.P.J. Barz, H. Farangis Zadeh, and P. Ehrhard, "Laminar flow and mass transport in a twice–folded microchannel," AIChE J. **54**, 381–393 (2008)

[32] D.P.J. Barz, H. Farangis Zadeh, and P. Ehrhard, "Flow fields within an electrokinetic micromixer," J. Fluid Mech. **676**, 265–293 (2011)

[33] M. van Dyke, *Perturbation Methods in Fluid Mechanics* (The Parabolic Press, Stanford, 1975)

[34] M v. Smoluchowski, "Contribution à la théorie de l'endosmose électrique et de quelques phenoménes corrélatifs," Bull. Int. Acad. Sci. Cracovie **8**, 182–200 (1903)

[35] H. Anzt, W. Augustin, M. Baumann, H. Bockelmann, T. Gengenbach, T. Hahn, V. Heuveline, E. Ketelaer, D. Lukarski, A. Otzen, S. Ritterbusch, B. Rocker, S. Ronnas, M. Schick, C. Subramanian, J.-P. Weiss, and F. Wilhelm, *HiFlow*^{3} *- A flexible and hardware-aware parallel finite element package*, Tech. Rep. No. 2010-06 (Preprint Series of the Engineering Mathematics and Computing Lab (EMCL) – Karlsruhe Institute of Technology, 2010)

[36] A. Guenther, M. Jhunjhunwala, M. Thalmann, M.A. Schmidt, and K.F. Jensen, "Micromixing of miscible liquids in segmented gas-liquid flow," Langmuir **21**, 1547–1555 (2005)

[37] H. Bockelmann, *High Performance Computing Based Methods for Simulation and Optimisation of Flow Problems*, Ph.D. thesis, , Fakultät für Mathematik, Universität Karlsruhe (2010)

[38] M. D. Gunzburger, *Perspectives in flow control and optimization* (SIAM, 2003)

[39] M.D. Gunzburger, "Adjoint equation-based methods for control problems in incompressible, viscous flows," Flow, Turbulence and Combustion **65**, 249–272 (2000)

[40] Karl Kunisch, *Optimal control of coupled systems of partial differential equations*, edited by G. Leugering, J. Sprekels, and F. Troeltzsch, International Series of Numerical Mathematics (Birkhaeuser Basel, Basel, 2009)

[41] F. Troeltzsch, *Optimal control of partial differential equations : theory, methods and applications*, Graduate studies in mathematics ; 112 (American Mathematical Society, Providence, RI, 2010)

Preprint Series of the Engineering Mathematics and Computing Lab

recent issues

No. 2012-01 Sven Janko, Björn Rocker, Martin Schindewolf, Vincent Heuveline, Wolfgang Karl: Software Transactional Memory, OpenMP and Pthread implementations of the Conjugate Gradients Method - a Preliminary Evaluation

No. 2011-17 Hartwig Anzt, Jack Dongarra, Vincent Heuveline, Piotr Luszczek: GPU-Accelerated Asynchronous Error Correction for Mixed Precision Iterative Refinement

No. 2011-16 Vincent Heuveline, Sebastian Ritterbusch, Staffan Ronnås: Augmented Reality for Urban Simulation Visualization

No. 2011-15 Hartwig Anzt, Jack Dongarra, Mark Gates, Stanimire Tomov: Block-asynchronous multigrid smoothers for GPU-accelerated systems

No. 2011-14 Hartwig Anzt, Jack Dongarra, Vincent Heuveline, Stanimire Tomov: A Block-Asynchronous Relaxation Method for Graphics Processing Units

No. 2011-13 Vincent Heuveline, Wolfgang Karl, Fabian Nowak, Mareike Schmidtobreick, Florian Wilhelm: Employing a High-Level Language for Porting Numerical Applications to Reconfigurable Hardware

No. 2011-12 Vincent Heuveline, Gudrun Thäter: Proceedings of the 4th EMCL-Workshop Numerical Simulation, Optimization and High Performance Computing

No. 2011-11 Thomas Gengenbach, Vincent Heuveline, Mathias J. Krause: Numerical Simulation of the Human Lung: A Two–scale Approach

No. 2011-10 Vincent Heuveline, Dimitar Lukarski, Fabian Oboril, Mehdi B. Tahoori, Jan-Philipp Weiss: Numerical Defect Correction as an Algorithm-Based Fault Tolerance Technique for Iterative Solvers

No. 2011-09 Vincent Heuveline, Dimitar Lukarski, Nico Trost, Jan-Philipp Weiss: Parallel Smoothers for Matrix-based Multigrid Methods on Unstructured Meshes Using Multicore CPUs and GPUs

No. 2011-08 Vincent Heuveline, Dimitar Lukarski, Jan-Philipp Weiss: Enhanced Parallel ILU(p)-based Preconditioners for Multi-core CPUs and GPUs – The Power(q)-pattern Method

No. 2011-07 Thomas Gengenbach, Vincent Heuveline, Rolf Mayer, Mathias J. Krause, Simon Zimny: A Preprocessing Approach for Innovative Patient-specific Intranasal Flow Simulations

No. 2011-06 Hartwig Anzt, Maribel Castillo, Juan C. Fernández, Vincent Heuveline, Francisco D. Igual, Rafael Mayo, Enrique S. Quintana-Ortí: Optimization of Power Consumption in the Iterative Solution of Sparse Linear Systems on Graphics Processors

No. 2011-05 Hartwig Anzt, Maribel Castillo, José I. Aliaga, Juan C. Fernández, Vincent Heuveline, Rafael Mayo, Enrique S. Quintana-Ortí: Analysis and Optimization of Power Consumption in the Iterative Solution of Sparse Linear Systems on Multi-core and Many-core Platforms

No. 2011-04 Vincent Heuveline, Michael Schick: A local time–dependent Generalized Polynomial Chaos method for Stochastic Dynamical Systems